



## Ca<sup>2+</sup> Sensitivity of Anoctamin 6/TMEM16F Is Regulated by the Putative Ca<sup>2+</sup>-Binding Reservoir at the N-Terminal Domain

Jae Won Roh<sup>1</sup>, Ga Eun Hwang<sup>1</sup>, Woo Kyung Kim<sup>2,3,\*</sup>, and Joo Hyun Nam<sup>1,3,\*</sup>

<sup>1</sup>Department of Physiology, Dongguk University College of Medicine, Gyeongju 38066, Korea, <sup>2</sup>Department of Internal Medicine, Graduate School of Medicine, Dongguk University, Goyang 10326, Korea, <sup>3</sup>Channelopathy Research Center (CRC), Dongguk University College of Medicine, Goyang 10326, Korea

\*Correspondence: wk2kim@naver.com (WKK); jhnam@dongguk.ac.kr (JHN)

<https://doi.org/10.14348/molcells.2021.2203>

[www.molcells.org](http://www.molcells.org)

Anoctamin 6/TMEM16F (ANO6) is a dual-function protein with Ca<sup>2+</sup>-activated ion channel and Ca<sup>2+</sup>-activated phospholipid scramblase activities, requiring a high intracellular Ca<sup>2+</sup> concentration (e.g., half-maximal effective Ca<sup>2+</sup> concentration [EC<sub>50</sub>] of [Ca<sup>2+</sup>]<sub>i</sub> > 10 μM), and strong and sustained depolarization above 0 mV. Structural comparison with Anoctamin 1/TMEM16A (ANO1), a canonical Ca<sup>2+</sup>-activated chloride channel exhibiting higher Ca<sup>2+</sup> sensitivity (EC<sub>50</sub> of 1 μM) than ANO6, suggested that a homologous Ca<sup>2+</sup>-transferring site in the N-terminal domain (Nt) might be responsible for the differential Ca<sup>2+</sup> sensitivity and kinetics of activation between ANO6 and ANO1. To elucidate the role of the putative Ca<sup>2+</sup>-transferring reservoir in the Nt (Nt-CaRes), we constructed an ANO6-1-6 chimera in which Nt-CaRes was replaced with the corresponding domain of ANO1. ANO6-1-6 showed higher sensitivity to Ca<sup>2+</sup> than ANO6. However, neither the speed of activation nor the voltage-dependence differed between ANO6 and ANO6-1-6. Molecular dynamics simulation revealed a reduced Ca<sup>2+</sup> interaction with Nt-CaRes in ANO6 than ANO6-1-6. Moreover, mutations on potentially Ca<sup>2+</sup>-interacting acidic amino acids in ANO6 Nt-CaRes resulted in reduced Ca<sup>2+</sup> sensitivity, implying direct interactions of Ca<sup>2+</sup> with these residues. Based on these results, we cautiously suggest that the net charge of Nt-CaRes is responsible for the difference in Ca<sup>2+</sup> sensitivity

between ANO1 and ANO6.

**Keywords:** anoctamin 6, calcium-binding domain, calcium sensitivity, TMEM16F

### INTRODUCTION

Anoctamin 6/TMEM16F (ANO6) is a dual-function protein with both calcium-activated ion channel and calcium-activated phospholipid scramblase activities (Kunzelmann et al., 2014; Suzuki et al., 2010; Whitlock and Hartzell, 2017). As a Ca<sup>2+</sup>-activated ion channel, ANO6 regulates full platelet activation and spinal motor neuron activity (Harper and Poole, 2013; Soulard et al., 2020). As a Ca<sup>2+</sup>-activated phospholipid scramblase, ANO6 also regulates blood coagulation, bone mineralization, plasma membrane repair, viral infection, and placental trophoblast fusion (Ehlen et al., 2013; Wu et al., 2020; Yang et al., 2012; Zaitseva et al., 2017; Zhang et al., 2020). However, the physiological mechanism linking these distinctly different functions remains unclear despite active investigations into the issue (Falzone et al., 2018; Kunzelmann et al., 2014; Pedemonte and Galietta, 2014).

Recent structural studies have revealed key insights into the mechanism of ANO6 activation. By comparing Ca<sup>2+</sup>-free

Received 14 October, 2020; revised 5 January, 2021; accepted 26 January, 2021; published online 25 February, 2021

eISSN: 0219-1032

©The Korean Society for Molecular and Cellular Biology. All rights reserved.

©This is an open-access article distributed under the terms of the Creative Commons Attribution-NonCommercial-ShareAlike 3.0 Unported License. To view a copy of this license, visit <http://creativecommons.org/licenses/by-nc-sa/3.0/>.

and Ca<sup>2+</sup>-bound structures, Brunner et al. (2014) and Alvadia et al. (2019) found that the Ca<sup>2+</sup>-binding site in the transmembrane domain is a feature that is highly conserved in all Anoctamin families. They also pointed out that a hinge-forming G615 residue in murine ANO6 was responsible for conformational changes upon Ca<sup>2+</sup>-binding. Moreover, Feng et al. (2019) identified murine ANO6 structures with phosphatidylinositol-(4, 5)-bisphosphate (PIP<sub>2</sub>), and proposed an out-of-groove lipid scrambling model with an intact ion channel pore. However, the specific mechanism by which positively charged Ca<sup>2+</sup> ions enter the Ca<sup>2+</sup>-binding site that is deeply embedded in hydrophobic transmembrane domains remains unclear.

With regard to the activation mechanisms, the crucial characteristic of ANO6 is the requirement of a very high concentration of intracellular Ca<sup>2+</sup> ([Ca<sup>2+</sup>]<sub>i</sub>); that is, ANO6 has lower Ca<sup>2+</sup> sensitivity than Anoctamin 1/TMEM16A (ANO1), a canonical Ca<sup>2+</sup>-activated chloride channel without a scramblase function (Caputo et al., 2008; Pedemonte and Galietta, 2014; Schroeder et al., 2008; Yang et al., 2008). ANO1 has a half-maximal effective Ca<sup>2+</sup> concentration (EC<sub>50</sub>) of around 1 μM, which is within the physiological range (Pedemonte and Galietta, 2014; Tak et al., 2019; Yang et al., 2008). By contrast, the EC<sub>50</sub> of [Ca<sup>2+</sup>]<sub>i</sub> for ANO6 is well above the physiological range at about 10 μM (Alvadia et al., 2019; Grubb et al., 2013; Scudieri et al., 2015; Ye et al., 2018). Despite this difference, structural comparison of Ca<sup>2+</sup>-bound structures at high resolution indicated high similarity between ANO1 and

ANO6, with a root mean square deviation (RMSD) of only around 1 Å (Alvadia et al., 2019). Therefore, it was proposed that another Ca<sup>2+</sup>-handling structure and molecular mechanism might be involved.

Tak et al. (2019) recently reported that an EF hand-like region in ANO1 could facilitate the entry of Ca<sup>2+</sup> to the Ca<sup>2+</sup>-binding site in hydrophobic transmembrane domains. In fact, a marked reduction in the Ca<sup>2+</sup> sensitivity of ANO1 was observed when the negatively charged amino acids in the EF hand-like region of the cytoplasmic N-terminal domain (Nt) were substituted with alanine. Mechanistically, it was proposed that the EF hand-like region serves as a transient Ca<sup>2+</sup>-binding reservoir and facilitates Ca<sup>2+</sup> migration between transmembrane domains.

Comparison of the amino acid sequences of the EF hand-like domains between ANO1 and ANO6 revealed three additional cationic residues (K251, R253, and R254) in ANO6 (Fig. 1A). This suggests that the less-negative electrostatic charges might affect the efficiency of initial Ca<sup>2+</sup>-containing and -transferring (i.e., a Ca<sup>2+</sup> reservoir-like role) to the Ca<sup>2+</sup>-binding site in the transmembrane domain. In other words, we hypothesized that the 10-fold lower Ca<sup>2+</sup> sensitivity of ANO6 than ANO1 might be due to the difference in the EF hand-like putative Ca<sup>2+</sup>-binding reservoir domain in the Nt (Nt-CaRes).

In this study, we aimed to test this hypothesis by investigating the Ca<sup>2+</sup>- and voltage-dependent activation of ANO6 and its chimeric mutant, which was constructed by replacing

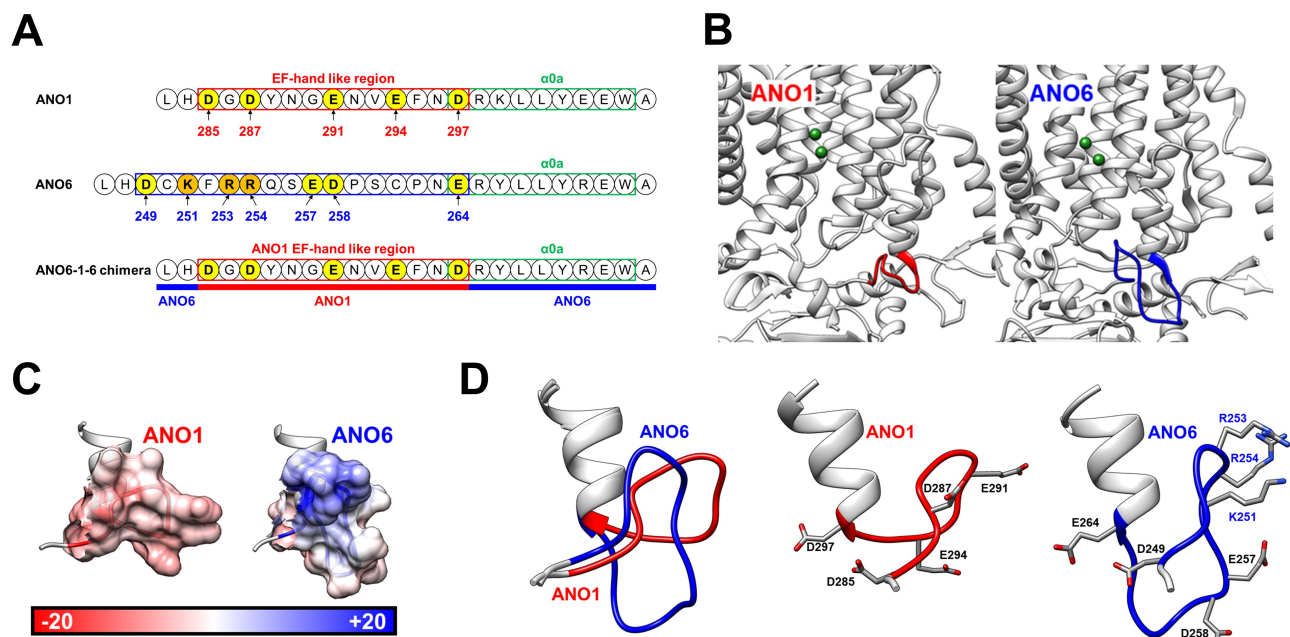


**Fig. 1. Identification of the sequence corresponding to the EF hand-like region in ANO6.** (A) Amino acid sequence alignment of human ANO1 and human ANO6 sequences. The EF hand-like region in ANO1 is indicated in the red box and the corresponding sequence in ANO6 is indicated in the blue box. The green box indicates the  $\alpha$ 0a helix. The ANO6-1-6 chimera was generated based on the sequence alignment. (B) Cryo-EM structures of human ANO1 (based on PDB ID 5OYG) and human ANO6 (based on PDB ID 6QPB). Ca<sup>2+</sup> (green sphere), the EF hand-like region in ANO1 (red loop), and the corresponding sequence in ANO6 (blue loop) are indicated. (C) Electrostatic surface potential of the EF hand-like region in ANO1 and the corresponding sequence in ANO6. (D) Overlaid structures of ANO1 (red loop) and ANO6 (blue loop). Acidic and basic amino acids are indicated.

the Nt-CaRes with the corresponding domain of ANO1. In addition to electrophysiological analysis using the patch-clamp technique, molecular dynamics (MD) simulations were performed to obtain further insight into the underlying activation mechanism of ANO6.

## MATERIALS AND METHODS

### Cell culture

HEK293T cells (American Type Culture Collection, USA) were cultured in high-glucose Dulbecco's modified Eagle's medium (Thermo Fisher Scientific, USA) supplemented with 10% fetal bovine serum (Thermo Fisher Scientific) and 1% penicillin/streptomycin (Thermo Fisher Scientific). The cells were cultured in a humidified incubator at 37°C with 20% O<sub>2</sub> and 10% CO<sub>2</sub>, and were subcultured every 2 days or 3 days. HEK293T cells were cultured in 6-well plates and 25-T flasks for electrophysiological experiments.

### Plasmids and transfection

A mammalian expression plasmid was used to express the human ANO6 (hANO6) V1 transcript (GenBank accession No. NM\_001025356.2). The ANO6-1-6 chimera (C250-E264\_GDYNGENVEFND), E257A mutation, E264A mutation, D249A\_E257A\_D258A\_E264A mutation, and K251A\_R253A\_R254A mutation were generated by Cosmo-Genetech (Seoul, Korea), and the sequences were confirmed through DNA sequencing. Plasmids were transiently transfected into HEK293T cells using Turbofect transfection reagent (Thermo Fisher Scientific) in accordance with the manufacturer's instructions. For electrophysiological experiments, HEK293T cells (cultured in 6-well plates) were co-transfected with 0.9 µg of ANO6 or mutant plasmid along with 0.1 µg of a green fluorescent protein expression plasmid to visualize the transfected cells. Experiments were performed within 24–36 h after transfection.

### Solutions

The whole-cell patch-clamp experiment was conducted using a basal extracellular solution containing 146 mM NaCl, 1 mM CaCl<sub>2</sub>, 1 mM MgCl<sub>2</sub>, 10 mM HEPES, and 10 mM glucose (adjusted to pH 7.4 with NaOH). The basal pipette solution contained 148.74 mM NaCl, 5 mM HEDTA, and 10 mM HEPES (adjusted to pH 7.2 with NaOH). An appropriate amount of CaCl<sub>2</sub> was added to the pipette solution to obtain a 10 µM free Ca<sup>2+</sup> concentration. This amount was calculated using WEBMAX-C software (C. Patton, Stanford University; <https://somapp.ucdmc.ucdavis.edu/pharmacology/bers/maxchelator/webmaxc/webmaxcS.htm>). Because CaCl<sub>2</sub> consists of two Cl<sup>-</sup> and one Ca<sup>2+</sup>, an appropriate amount of NaCl was added to the basal pipette solution to adjust the Cl<sup>-</sup> concentration to 150 mM.

For the inside-out patch-clamp experiment, the basal pipette solution contained 146 mM NaCl, 1 mM CaCl<sub>2</sub>, 1 mM MgCl<sub>2</sub>, 10 mM HEPES, and 10 mM glucose (adjusted to pH 7.4 with NaOH). The bath solution for the intracellular side of the patch contained 150 mM NaCl, 1 mM HEDTA, and 10 mM HEPES (adjusted to pH 7.2 with NaOH). To obtain different concentrations of free Ca<sup>2+</sup>, an appropriate amount

of CaCl<sub>2</sub> was added to obtain free Ca<sup>2+</sup> concentrations of 3, 6, 10, 17, 30, 100, and 300 µM, respectively. To prepare solutions with a free Ca<sup>2+</sup> concentration higher than 100 µM, appropriate amounts of NaCl and CaCl<sub>2</sub> were added to reach a 150 mM Cl<sup>-</sup> concentration.

### Electrophysiology

The whole-cell and inside-out patch-clamp methods were used to measure the channel activities of ANO6-transfected HEK293T cells at 25°C. The cells were transferred to a bath, perfused at 10 ml/min at room temperature, and mounted on the stage of an inverted microscope (Ti-U; Nikon, Japan) equipped with a high-density mercury lamp light source for green fluorescence excitation. Microglass pipettes (World Precision Instruments, USA) were fabricated using a PP-830 single-stage glass microelectrode puller (Narishige, Japan) with a resistance of 2-3 MΩ and 3-5 MΩ for the whole-cell and inside-out patch recordings, respectively. The liquid junction potential was rectified with an offset circuit before each experiment. Currents were recorded using an Axopatch 200B amplifier and Digidata 1440A interface, digitized at 10 kHz and low-pass filtered at 5 kHz with pClamp software 10.7 (Molecular Devices, USA). In the whole-cell patch-clamp configuration, a ramp-like pulse from -100 mV to +100 mV (duration time 3 s) was applied every 20 s with 0-mV holding voltage, and the inside-out patch recordings were obtained at a holding voltage of +80 mV.

### Data analysis

To calculate the EC<sub>50</sub> of Ca<sup>2+</sup>, currents recorded in the inside-out patch-clamp configuration were normalized and then fitted to the Hill equation as follows:

$$\frac{I}{I_{max}} = \frac{1}{1 + \left[ \frac{(EC_{50})}{[Ca^{2+}]} \right]^H}$$

where I/I<sub>max</sub> is the normalized current, EC<sub>50</sub> is the half-maximal effective concentration of Ca<sup>2+</sup>, Ca<sup>2+</sup> is the free Ca<sup>2+</sup> concentration, and H is the Hill coefficient.

To calculate the half-maximal effective voltage (V<sub>50</sub>), conductance values recorded in the inside-out patch-clamp configuration were normalized and then fitted to the Boltzmann equation as follows:

$$\frac{G}{G_{max}} = \frac{1}{1 + e^{\frac{-zF(V_m - V_{50})}{RT}}}$$

where G/G<sub>max</sub> is the normalized conductance, V<sub>m</sub> is the membrane voltage, V<sub>50</sub> is the half-maximal effective voltage, z is the charge of the gating ions, F is Faraday's constant, R is the gas constant, and T is the absolute temperature.

### Determination of ANO6 structure

The cryogenic-electron microscopy (cryo-EM) structure of Ca<sup>2+</sup>-free murine ANO6 at a 3.60 Å resolution (Protein Data Bank [PDB] ID 6QPB) (Alvadia et al., 2019) was used as a template for MD simulations. Since human ANO6 variant 1 was used throughout this study, the murine ANO6 structure was changed to the human ANO6 variant 1 sequence using the SWISS MODEL homology-modeling server (Schwede et al., 2003). Missing loops were automatically generated, except for the highly variable Nt and C-terminal residues. For

the ANO6-1-6 chimera (C250-E264\_GDYNGENVEFND), the cryo-EM structure of the Ca<sup>2+</sup>-free murine ANO1 structure at a 4.06 Å resolution (PDB ID 5OYG) (Paulino et al., 2017) was considered because the chimera sequence (GDYNGENVEFND) was the same as the corresponding human ANO1 sequence. The structure of murine ANO1 was then altered to the ANO6-1-6 sequence through the SWISS MODEL homology-modeling server (Schwede et al., 2003). The modeling results for ANO6 and ANO6-1-6 showed a qualitative model energy analysis (QMEAN) score of -2.99 and -4.74, respectively (Berkert et al., 2009). Nt-CaRes and the α<sub>0</sub>α helix were included in the MD simulations, corresponding to residues L247-A273 in the human ANO6 sequence.

### Molecular dynamics simulation

The protein structure was first solvated using the CHARMM-GUI web server (Lee et al., 2016). While solvating with TIP3P water molecules, CaCl<sub>2</sub> was added at an appropriate concentration to include eight to nine Ca<sup>2+</sup> ions via the Monte Carlo ion placing method (Jorgensen et al., 1983). The final system included the protein structure and ~3,000 TIP3P water molecules, with ~10,000 atoms in a 48 × 48 × 48 Å<sup>3</sup> box.

All simulations were carried out using the CHARMM36m force field (Huang et al., 2017) and CUDA-enabled NAMD 2.14 (Phillips et al., 2005). The particle mesh Ewald algorithm was used to evaluate long-distance electrostatic interactions (Darden et al., 1993). Van der Waals interactions for a smoothing function were considered from 10 to 12 Å. Complete electronic evaluations were performed every 2 fs using the SHAKE algorithm (Ryckaert et al., 1977). The pressure and temperature were maintained at 1 atm and 310 K throughout the simulation, using the Nosé–Hoover Langevin piston method and Langevin dynamics, respectively (Hoover, 1985; Nosé, 1984). Anisotropic cell fluctuations were not observed.

The system was first minimized for 10,000 steps. Thereafter, a 1-ns simulation was performed with 1,000,000 steps. Snapshots were saved every 100 steps to evaluate the system. After the simulation, distances between the protein and Ca<sup>2+</sup> were analyzed using visual molecular dynamics (VMD) (Humphrey et al., 1996). For both ANO6 and ANO6-1-6, 10 simulations were carried out. Independent systems containing different initial ion placements were generated for each simulation. All structural figures were generated using UCSF Chimera (Pettersen et al., 2004).

### Statistical analysis

The data are expressed as mean ± SEM values. Student's *t*-tests were performed to compare independent control and experimental groups. For multiple-group comparisons, one-way analysis of variance (ANOVA) with Tukey's post-hoc tests were performed. *P* values less than 0.05 were considered statistically significant. All statistical analysis were made using pClamp (ver. 10.7; Molecular Devices, USA), OriginLab (ver. 9.0; OriginLab Corporation, USA), and GraphPad Prism (ver. 8.0.1; GraphPad Software, USA).

## RESULTS

### Identification of the sequence corresponding to the EF hand-like region in ANO6

Based on the results of Tak et al. (2019), we aligned the sequence of ANO6 corresponding to the EF hand-like region in ANO1 (Fig. 1A). The EF hand-like region in ANO1 contains five negatively charged residues (D285, D287, E291, E294, and D297) without cationic amino acids. In contrast, the corresponding region in ANO6 contains four anionic residues (D249, E257, D258, and E264) and three cationic residues (K251, R253, and R254).

The locations of the EF hand-like sequence in the cryo-EM structure were similar between ANO1 and ANO6, relatively close to the Ca<sup>2+</sup>-binding site (Fig. 1B), with distances of about 18 Å in both cases. However, the electrostatic surface potentials of these sequences were quite different; ANO1 is negatively charged and ANO6 is partially positively charged owing to its basic amino acids (K251, R253, and R254) (Figs. 1A and 1C). Overlaying the corresponding structures of ANO1 and ANO6 more clearly revealed the structural differences (Fig. 1D). The RMSD between the two structures was about 2.60 Å. As we were primarily interested in the similarities and differences of the EF hand-like sequence compared with that of ANO1, we decided to investigate its role as a “putative” Ca<sup>2+</sup>-binding reservoir (Nt-CaRes) in ANO6.

### ANO6-1-6 shows higher Ca<sup>2+</sup> sensitivity than ANO6

We constructed the ANO6-1-6 chimera, in which the Nt-CaRes of ANO6 was replaced by that of ANO1 (Fig. 1A). In the whole-cell patch-clamp experiments of HEK293T cells overexpressing the two clones, ramp-like depolarizing pulses were repetitively applied to investigate the activation of ANO6 and ANO6-1-6 current. After membrane break-in (i.e., whole-cell configuration with a 0 μM or 10 μM Ca<sup>2+</sup> concentration in the pipette solution), a slow increase of membrane conductance with an outwardly rectifying property was observed in 10 μM Ca<sup>2+</sup> but not in 0 μM Ca<sup>2+</sup>, indicating Ca<sup>2+</sup>-dependent activation (Figs. 2A and 2B). The peak amplitude of the outward current was clearly higher in ANO6-1-6 (217.5 ± 55.6 pA/pF) than in ANO6 (65.4 ± 14.6 pA/pF) at 10 μM Ca<sup>2+</sup> (Fig. 2C). However, the currents at 0 μM Ca<sup>2+</sup> were not significantly different in ANO6 (9.1 ± 2.4 pA/pF) and ANO6-1-6 (8.5 ± 1.6 pA/pF) (Fig. 2C). The time to reach the peak amplitude with the whole-cell configuration did not differ between the wild-type and chimera protein, at 520.0 ± 43.0 s and 568.0 ± 53.5 s, respectively (Fig. 2D). After reaching the peak amplitude, a spontaneous partial decrease of the current (i.e., inactivation) was observed. The normalized rate of inactivation ( $I/I_{max}$ ) was not different between ANO6 (0.88 ± 0.05) and ANO6-1-6 (0.89 ± 0.08) at 60 s after the peak (Fig. 2E).

The precise Ca<sup>2+</sup> sensitivity of ANO6 and ANO6-1-6 were investigated using the inside-out patch-clamp technique. Various levels of [Ca<sup>2+</sup>]<sub>i</sub> could be directly applied to the cytoplasmic side of the patch membrane, and the concentration-dependent activation of outward currents could be elicited reversibly (Figs. 2F and 2G). The EC<sub>50</sub> values were 11.64 μM (Hill coefficient = 3.99) and 6.68 μM (Hill coefficient = 3.42)

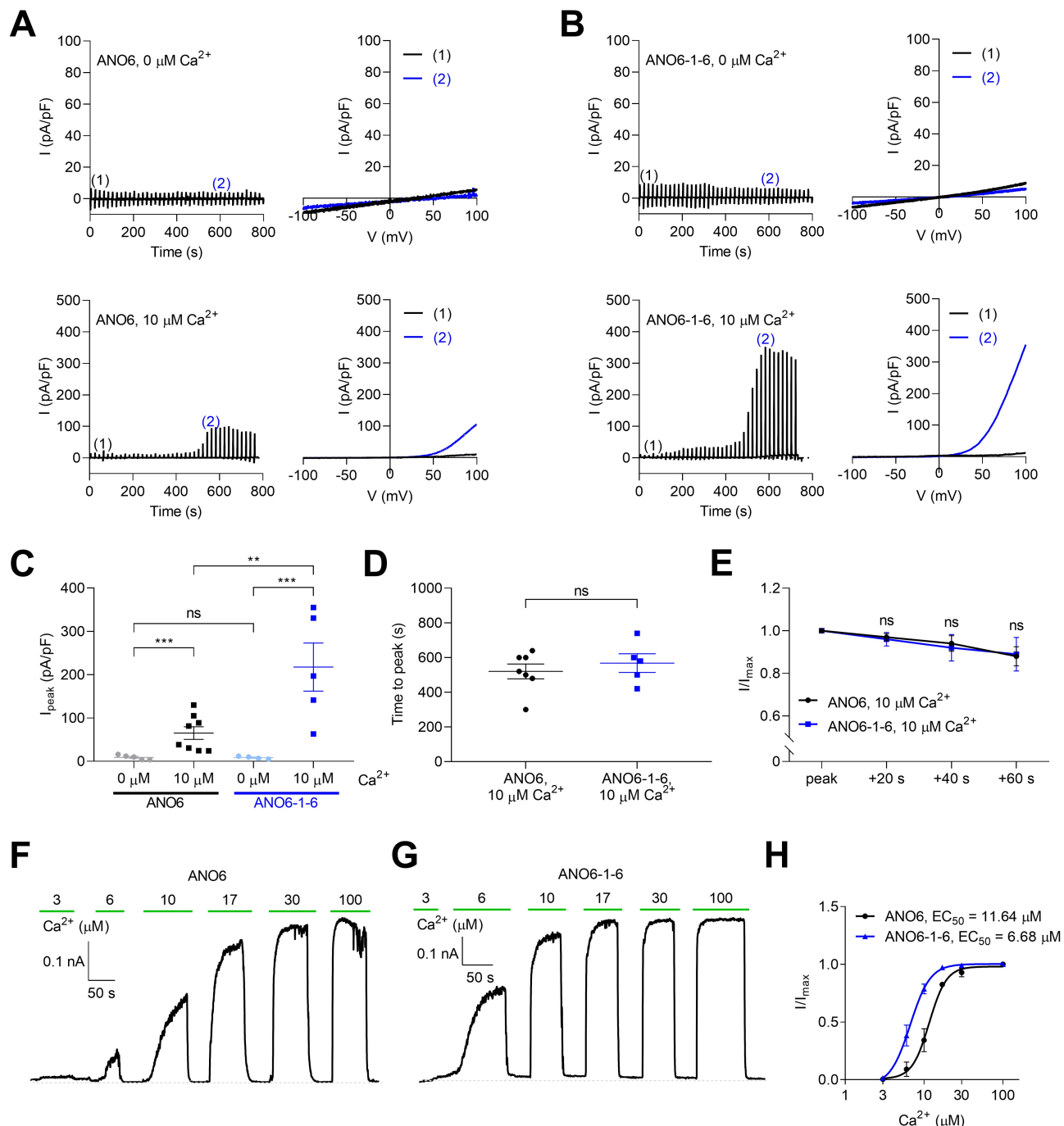


**Fig. 2. ANO6-1-6 shows higher  $\text{Ca}^{2+}$  sensitivity than ANO6.** (A and B) Current traces of ANO6 and ANO6-1-6 in the whole-cell patch clamp. The holding voltage was 0 mV and ramp-like pulses from -100 to +100 mV were applied every 20 s with a 3-s duration. The free  $\text{Ca}^{2+}$  concentrations were 0  $\mu\text{M}$  and 10  $\mu\text{M}$  for ANO6 and ANO6-1-6. (C) Maximal current comparison of ANO6 and ANO6-1-6 currents in the whole-cell patch clamp ( $n = 5$  for ANO6 at 0  $\mu\text{M}$   $\text{Ca}^{2+}$ ,  $n = 8$  for ANO6 at 10  $\mu\text{M}$   $\text{Ca}^{2+}$ ,  $n = 4$  for ANO6-1-6 at 0  $\mu\text{M}$   $\text{Ca}^{2+}$ , and  $n = 5$  for ANO6-1-6 at 10  $\mu\text{M}$   $\text{Ca}^{2+}$ ). (D) Time-to-peak comparison of ANO6 and ANO6-1-6 currents in the whole-cell patch clamp ( $n = 7$  for ANO6 at 10  $\mu\text{M}$   $\text{Ca}^{2+}$  and  $n = 5$  for ANO6-1-6 at 10  $\mu\text{M}$   $\text{Ca}^{2+}$ ). (E) Comparison of ANO6 and ANO6-1-6 channel inactivation by normalized currents in the whole-cell patch clamp ( $n = 5$  for ANO6 at 10  $\mu\text{M}$   $\text{Ca}^{2+}$  and  $n = 4$  for ANO6-1-6 at 10  $\mu\text{M}$   $\text{Ca}^{2+}$ ). (F and G) Current traces of ANO6 and ANO6-1-6 in the inside-out patch clamp. The holding voltage was +80 mV and applied free  $\text{Ca}^{2+}$  concentrations are indicated. Gray dotted lines indicate 0 pA. (H) Comparison of  $\text{Ca}^{2+}$  sensitivity of ANO6 and ANO6-1-6 in the inside-out patch clamp ( $n = 4$  for ANO6 and  $n = 4$  for ANO6-1-6). The Hill equation was used to calculate  $\text{EC}_{50}$ . All values in (C, D, E, and H) are expressed as mean  $\pm$  SEM. The  $P$  values in (C) were calculated by one-way ANOVA with Tukey's post-hoc tests for each column. The  $P$  values in (D and E) were calculated by Student's  $t$ -tests. ns, not significant. \*\* $P < 0.01$ , \*\*\* $P < 0.001$ .

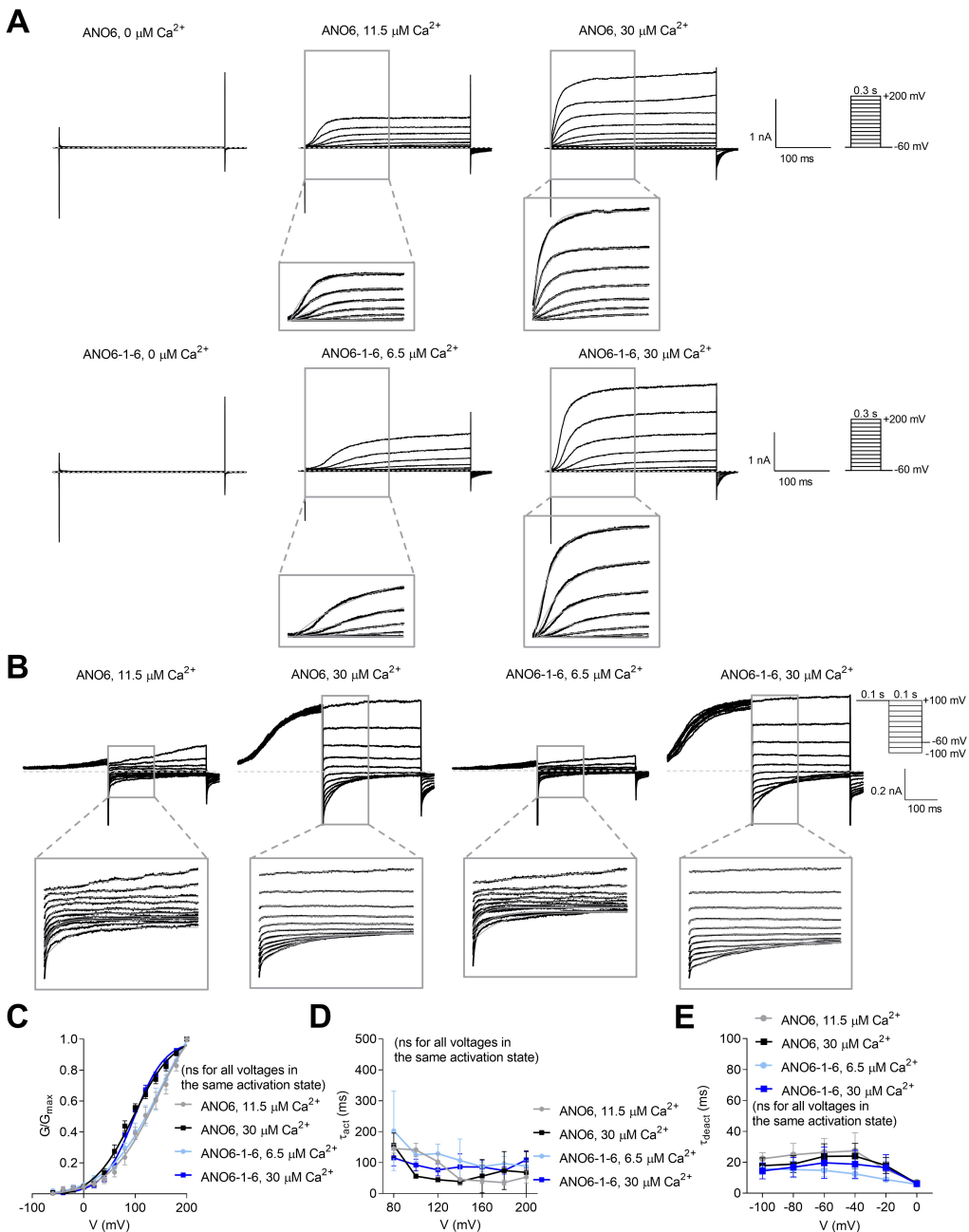


**Fig. 3. ANO6 and ANO6-1-6 show no difference in voltage dependence.** (A) Current traces of ANO6 and ANO6-1-6 in the inside-out patch clamp. The free  $\text{Ca}^{2+}$  concentrations are indicated above each graph. The step pulse was administered from -60 to +200 mV with +20-mV increments and was held at -60 mV. Gray dotted lines indicate 0 pA. In magnified images, gray lines are the fitted single exponential curves. (B) Current traces of ANO6 and ANO6-1-6 in the inside-out patch clamp. Initially, a +100-mV pulse was applied to activate the channel at a specific  $\text{Ca}^{2+}$  concentration, and voltage was applied from -100 to +100 mV with +20-mV increments and was held at -60 mV. Gray dotted lines indicate 0 pA. In magnified images, gray lines are the fitted single exponential curves. (C) Comparison of voltage-dependent conductance of ANO6 and ANO6-1-6 currents. Channel conductance was assessed from the magnitude of tail currents from (A). After normalizing to the conductance at +200 mV, the Boltzmann equation was used to calculate  $V_{50}$  ( $n = 5$  for ANO6 at 11.5  $\mu\text{M}$   $\text{Ca}^{2+}$ ,  $n = 8$  for ANO6 at 30  $\mu\text{M}$   $\text{Ca}^{2+}$ ,  $n = 8$  for ANO6-1-6 at 6.5  $\mu\text{M}$   $\text{Ca}^{2+}$ , and  $n = 5$  for ANO6-1-6 at 30  $\mu\text{M}$   $\text{Ca}^{2+}$ ). (D) Activation time constant analysis of ANO6 and ANO6-1-6. A single exponential fitting was conducted for activating currents from (A) ( $n = 5$  for ANO6 at 11.5  $\mu\text{M}$   $\text{Ca}^{2+}$ ,  $n = 8$  for ANO6 at 30  $\mu\text{M}$   $\text{Ca}^{2+}$ ,  $n = 8$  for ANO6-1-6 at 6.5  $\mu\text{M}$   $\text{Ca}^{2+}$ , and  $n = 5$  for ANO6-1-6 at 30  $\mu\text{M}$   $\text{Ca}^{2+}$ ). (E) Deactivation time constant analysis of ANO6 and ANO6-1-6. Single exponential fitting was performed for tail currents shown in (B) ( $n = 6$  for ANO6 at 11.5  $\mu\text{M}$   $\text{Ca}^{2+}$ ,  $n = 6$  for ANO6 at 30  $\mu\text{M}$   $\text{Ca}^{2+}$ ,  $n = 7$  for ANO6-1-6 at 6.5  $\mu\text{M}$   $\text{Ca}^{2+}$ , and  $n = 7$  for ANO6-1-6 at 30  $\mu\text{M}$   $\text{Ca}^{2+}$ ). All values in (C, D, and E) are expressed as mean  $\pm$  SEM. The  $P$  values in (C, D, and E) were calculated by one-way ANOVA with Tukey's post-hoc tests for each column. ns, not significant.

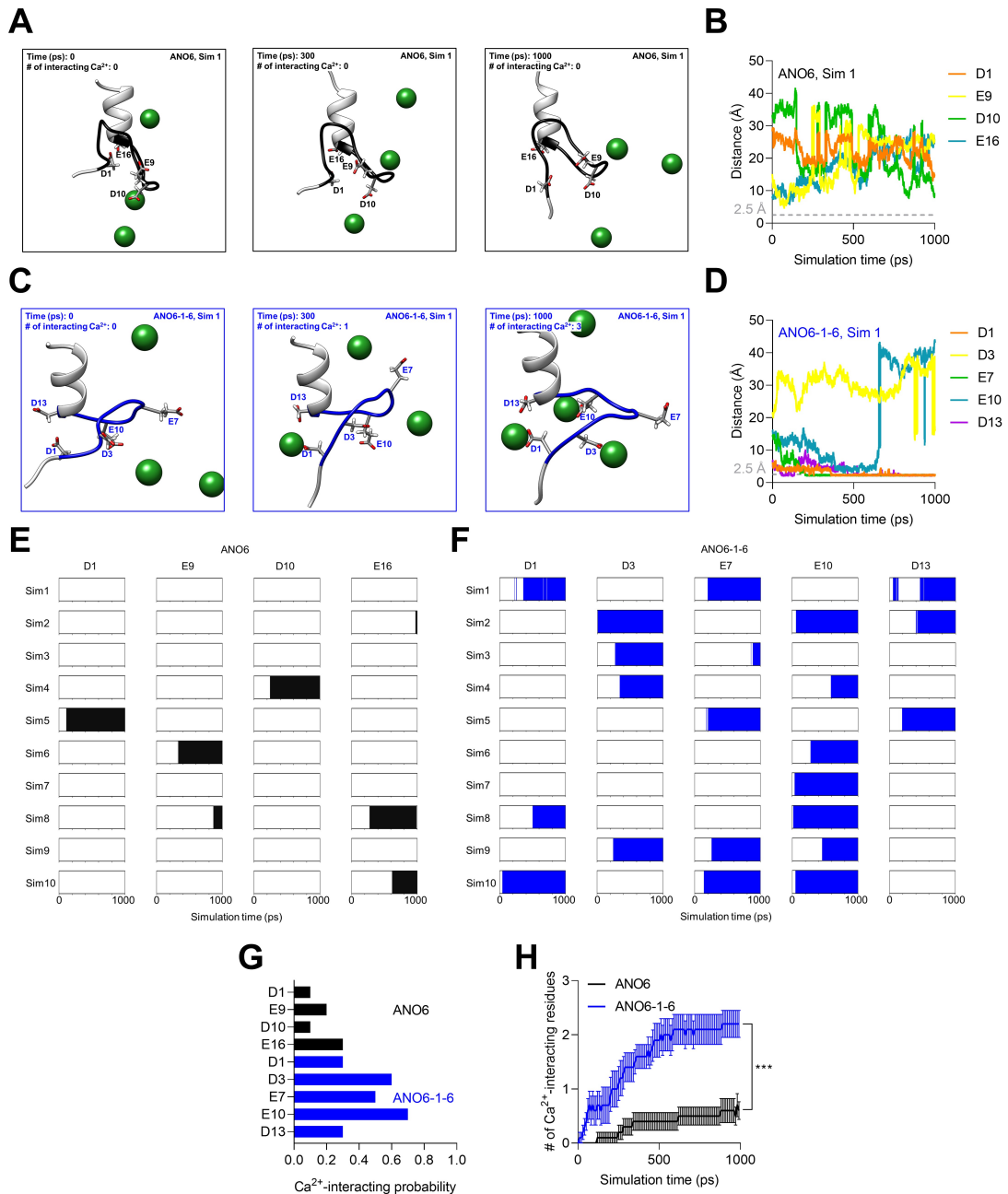


**Fig. 4. Molecular dynamics simulations of Nt-CaRes movement.** (A) Snapshots of ANO6 at 0, 300, and 1,000 ps from the molecular dynamics simulation. Amino acid letters indicate relative acidic amino acid positions in the “putative” Ca<sup>2+</sup>-binding reservoir in ANO6, which is 1DCKFRRQSEDPSCPNE16. The putative Ca<sup>2+</sup>-binding reservoir in ANO6 (black loop), Ca<sup>2+</sup> (green sphere), simulation time, and the number of interacting Ca<sup>2+</sup> molecules are indicated. No interacting Ca<sup>2+</sup> was noted. (B) Time-distance graph of ANO6 simulation. Distances represent the distance between the oxygen atom in the acidic amino acid to the nearest Ca<sup>2+</sup>. The stable interaction length was calculated as 2.5 Å (gray dotted line). (C) Snapshots of ANO6-1-6 at 0, 300, and 1,000 ps from the molecular dynamics simulation. Amino acid letters indicate relative acidic amino acid positions in the putative Ca<sup>2+</sup>-binding reservoir in ANO6-1-6, which is 1DGDDYNGENVFND13. The Ca<sup>2+</sup>-binding reservoir in ANO6-1-6 (blue loop), Ca<sup>2+</sup> (green sphere), simulation time, and the number of interacting Ca<sup>2+</sup> ions are indicated. At 300 ps, D1 was shown to interact with Ca<sup>2+</sup>. At 1,000 ps, D1, D3, and E10 demonstrated interactions. (D) Time-distance graph of the ANO6-1-6 simulation. Distances represent the distance between the oxygen atom in the acidic amino acid to the nearest Ca<sup>2+</sup>. The stable interaction strength was calculated as 2.5 Å (gray dotted line). (E and F) Total result of 20 simulations, 10 for ANO6 and ANO6-1-6 each. Ca<sup>2+</sup>-binding to the reservoir is indicated with vertical lines. (G) Ca<sup>2+</sup>-interacting probability of the putative Ca<sup>2+</sup>-binding reservoirs in ANO6 and ANO6-1-6 (n = 10 ANO6 and n = 10 for ANO6-1-6). (H) The number of Ca<sup>2+</sup>-interacting residues during simulations. The P value was calculated after complete simulation (n = 10 for ANO6 and n = 10 for ANO6-1-6). All values in (H) are expressed as mean ± SEM. The P value in (H) was calculated by Student's t-test. \*\*\*P < 0.001.

for ANO6 and ANO6-1-6, respectively, indicating increased Ca<sup>2+</sup> sensitivity of ANO6-1-6 compared with ANO6 (Fig. 2H).

### ANO6 and ANO6-1-6 show no difference in voltage dependence

ANO6 activation requires membrane depolarization as well as a high [Ca<sup>2+</sup>]<sub>i</sub> (Alvadia et al., 2019; Yang et al., 2012; Ye et al., 2018). To compare the steady-state voltage dependence of the two forms of ANO6, a step-like pulse protocol was applied in the inside-out patch-clamp experiment. For the full activation of ANO6 and ANO6-1-6, 30 μM Ca<sup>2+</sup> was commonly used. In addition, to compare the voltage dependence at the EC<sub>50</sub> level of [Ca<sup>2+</sup>]<sub>i</sub>, we also conducted the patch-clamp experiment with 11.5 μM and 6.5 μM of [Ca<sup>2+</sup>]<sub>i</sub> for ANO6 and ANO6-1-6, respectively.

Voltage steps from -60 mV to +200 mV (duration time 0.3 s) were used to observe the activation kinetics. The common repolarization to -60 mV induced inward tail currents reflecting the deactivation process (Fig. 3A). For calculating inactivation kinetics and tail currents, a common strong depolarization (+100 mV, 0.1 s) was initially applied, followed by the application of various voltage steps from -100 mV to +100 mV (Fig. 3B). The voltage-dependent increase in membrane conductance (i.e., channel activation state) was calculated from the normalized magnitude of tail currents from Fig. 3A (Fig. 3C). The V<sub>50</sub> values were 142.0 mV and 96.4 mV for 11.5 μM and 30 μM Ca<sup>2+</sup> in ANO6, respectively, and were 147.2 mV and 98.1 mV for 6.5 μM and 30 μM Ca<sup>2+</sup> in ANO6-1-6, respectively. No significant differences were observed between ANO6 and ANO6-1-6 at 30 μM and the EC<sub>50</sub> (11.5 μM and 6.5 μM, respectively). The time constants of slow activation on membrane depolarizations were calculated by fitting the activating phase of currents to single exponential curves (Fig. 3D). The deactivation time constants were also calculated by fitting the tail currents to single exponential curves (Figs. 3B and 3E). No significant differences were observed in either activation or deactivation time constants. These results indicate that the voltage dependency of the channel remained unchanged in ANO6-1-6 compared with that of ANO6.

### MD simulations of Nt-CaRes movement

Next, we aimed to observe, albeit virtually, the function of the Nt-CaRes in ANO6 and ANO6-1-6 using MD simulations. Because no differences between ANO6 and ANO6-1-6 were observed other than Ca<sup>2+</sup> sensitivity in the patch-clamp experiments, we focused only on the interactions of the Nt-CaRes with Ca<sup>2+</sup>. The structures of the Nt-CaRes were generated using the SWISS MODEL homology-modeling server (PDB ID 6QPB for ANO6 and 5OYG for ANO6-1-6) (Alvadia et al., 2019; Paulino et al., 2017; Schwede et al., 2003). The total simulation system included a few sequences surrounding the Nt-CaRes. Eight to nine Ca<sup>2+</sup> molecules were placed evenly throughout the system. Ca<sup>2+</sup> interactions with the protein were confirmed when the distance between Ca<sup>2+</sup> and oxygen atoms in acidic amino acids was less than 2.5 Å, which represents the sum of oxygen and calcium atom radii. Each MD simulation lasted for 1 ns.

In the first simulation of ANO6, no interacting Ca<sup>2+</sup> was

observed (Figs. 4A and 4B), whereas in ANO6-1-6, three interacting Ca<sup>2+</sup> atoms were observed (Figs. 4C and 4D). To exclude potential effects of the initial distances between Ca<sup>2+</sup> and the acidic amino acids, we performed nine more independent simulations for ANO6 and ANO6-1-6. Ca<sup>2+</sup> molecules were randomly placed in each simulation, and a total of 20 MD simulations, 10 for each ANO6 and ANO6-1-6, were carried out (Figs. 4E and 4F). Consistently, Ca<sup>2+</sup> interactions occurred more frequently with ANO6-1-6 than with ANO6, regardless of the initial Ca<sup>2+</sup> positions. To determine the interaction affinity for each acidic amino acid in the Nt-CaRes, the Ca<sup>2+</sup>-interacting probability was calculated (Fig. 4G). Furthermore, the numbers of Ca<sup>2+</sup>-interacting residues in ANO6 and ANO6-1-6 were compared (Fig. 4H). Both the Ca<sup>2+</sup>-interacting probability and the number of Ca<sup>2+</sup>-interacting residues were higher in ANO6-1-6 than in ANO6. Therefore, the MD simulations showed that Ca<sup>2+</sup> interacted much better with the Nt-CaRes in ANO6-1-6 than in ANO6, which was in line with the higher Ca<sup>2+</sup> sensitivity of ANO6-1-6 observed in the patch-clamp experiments.

### Mutations in Nt-CaRes in ANO6 decrease Ca<sup>2+</sup> sensitivity

To ensure direct Ca<sup>2+</sup> binding to the Nt-CaRes in ANO6, we conducted site-directed mutagenesis experiments. Acidic amino acids with high Ca<sup>2+</sup> interaction probabilities were selected based on the results from the MD simulations, which were E257 and E264 (E9 and E16 in Fig. 4, respectively), which were individually substituted with alanine (E257A and E264A). In addition, we constructed a quadruple 4A mutation (D249A\_E257A\_D258A\_E264A) and a triple 3A mutation (K251A\_R253A\_R254A). In the inside-out patch-clamp experiment of the above four mutants, the EC<sub>50</sub> of [Ca<sup>2+</sup>]<sub>i</sub> was 18.18 μM for E257A (Hill coefficient = 3.04), 22.00 μM for E264A (Hill coefficient = 3.08), 77.78 μM for D249A\_E257A\_D258A\_E264A (4A, Hill coefficient = 1.40), and 10.03 μM for K251A\_R253A\_R254A (3A, Hill coefficient = 3.46), showing a significant decrease in Ca<sup>2+</sup> sensitivity for the E257A, E264A, and 4A mutants (Fig. 5).

## DISCUSSION

Our present study demonstrated the functional implication of the Nt domain of ANO6 corresponding to the Nt-CaRes of ANO1, suggesting that the less negative surface charge of the ANO6 Nt-CaRes could be responsible for the much lower Ca<sup>2+</sup> sensitivity of ANO6 than that of the canonical Ca<sup>2+</sup>-activated Cl<sup>-</sup> channel ANO1. Two lines of experimental evidence support the above interpretation: (1) the chimeric mutation replacing the Nt-CaRes with that of ANO1 significantly improved Ca<sup>2+</sup> sensitivity, and (2) neutralization of the anionic residue in the ANO6 Nt-CaRes reduced the Ca<sup>2+</sup> sensitivity. In addition, the MD simulation of the Nt-CaRes revealed much lower Ca<sup>2+</sup>-interacting kinetics of ANO6 than ANO1. These results may provide clues to answer the key question of the structural difference responsible for the lower Ca<sup>2+</sup> sensitivity of ANO6 than ANO1.

According to a very recent study of ANO1, the Ca<sup>2+</sup>-binding reservoir (Nt-CaRes) facilitates Ca<sup>2+</sup> movement or migration to the critical Ca<sup>2+</sup>-binding site in transmembrane

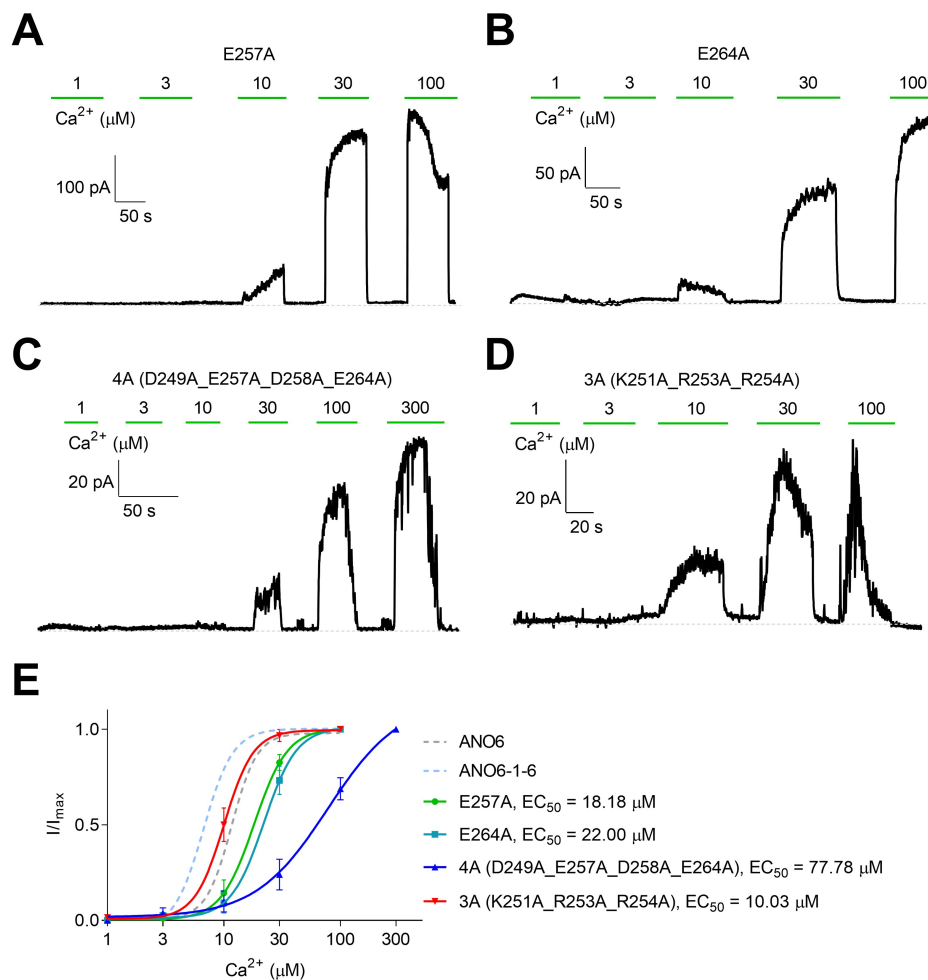


**Fig. 5. Mutations in Nt-CaRes in ANO6 decrease Ca<sup>2+</sup> sensitivity.**  
(A-D) Current traces of ANO6 mutations in the inside-out patch clamp. (A) E257A mutation, (B) E264A mutation, (C) D249A\_E257A\_D258A\_E264A mutation (4A), and (D) K251A\_R253A\_R254A mutation (3A). The holding voltage was +80 mV and the applied free Ca<sup>2+</sup> concentrations are indicated. Gray dotted lines indicate 0 pA. (D) Comparison of Ca<sup>2+</sup> sensitivity of ANO6, ANO6-1-6, and the E257A, E264A, 4A, and 3A mutants in the inside-out patch clamp (n = 6 for E257A, n = 5 for E264A, n = 6 for 4A, and n = 6 for 3A). The Hill equation was used to calculate EC<sub>50</sub>. All values in (E) are expressed as mean  $\pm$  SEM.

domains (Tak et al., 2019). Despite the similar location near the Ca<sup>2+</sup>-binding site, the corresponding region in ANO6 has a different surface charge due to the cationic residues (K251, R253, and R254). The site-directed mutation experiments of negative residues showed decreased Ca<sup>2+</sup> sensitivity, implying direct Ca<sup>2+</sup> interactions with these residues. In addition, the decreased Hill coefficients of the mutants (3.06 for E257A, 3.24 for E264A, and 1.54 for D249A\_E257A\_D258A\_E264A) compared to wild-type ANO6 (3.986) suggested less cooperative Ca<sup>2+</sup> interactions (Fig. 5E). Thus, we cautiously propose the investigated region in ANO6 as the Ca<sup>2+</sup>-binding reservoir, which helps Ca<sup>2+</sup> move to the Ca<sup>2+</sup>-binding site in hydrophobic transmembrane domains and is also responsible for the reduced Ca<sup>2+</sup> affinity relative to that of ANO1. However, we did not observe a difference in Ca<sup>2+</sup> sensitivity between ANO6 (EC<sub>50</sub> = 11.64  $\mu$ M) and the K251A\_R253A\_R254A mutant (EC<sub>50</sub> = 10.03  $\mu$ M). This could be because Ca<sup>2+</sup>-interacting negative residues may not be affected by positive charges from K251, R253, and R254, or that factors other than electrostatic charges could be responsible for Ca<sup>2+</sup> sensitivity.

Although major differences in Ca<sup>2+</sup> sensitivity were observed between ANO6 and ANO6-1-6, the voltage dependency remained unchanged (Fig. 2). Of note, the currents

did not saturate even at a very high voltage (i.e., +200 mV). Thus, calculating V<sub>50</sub> from unsaturated currents using the Boltzmann equation could be inaccurate in the absence of current saturation. Although the V<sub>50</sub> values were similar at the same activation states for ANO6 and ANO6-1-6 (142.0 mV and 96.4 mV for 11.5  $\mu$ M and 30  $\mu$ M Ca<sup>2+</sup> in ANO6, and 147.2 mV and 98.1 mV for 6.5  $\mu$ M and 30  $\mu$ M Ca<sup>2+</sup> in ANO6-1-6), extra caution in interpreting these values directly is required.

Tak et al. (2019) reported that the Ca<sup>2+</sup>-binding reservoir in ANO1 had a conserved sequence similar to that of EF hand-like domains. However, because this region in ANO1 did not exist in pairs and the three-dimensional structure was different from that of currently known EF-hand domains, its function as a “true” EF-hand domain was considered unlikely (Tak et al., 2019). The corresponding sequence in ANO6 cannot be considered as the EF-hand like domain owing to the presence of acidic amino acid residues in the 1st, 9th, 10th, and 16th positions, whereas in the conserved EF-hand domain, the 1st, 3rd, 5th, 9th, and 12th amino acid residues are acidic (Grabarek, 2006). Despite the low similarity to conventional EF-hand domains, the Nt-CaRes in ANO1 and ANO6 may bind Ca<sup>2+</sup> in unconventional forms with weak and transient interactions, which could explain why Ca<sup>2+</sup> binding to these

regions was not observed in structural analyses (Alvadia et al., 2019; Dang et al., 2017; Feng et al., 2019; Paulino et al., 2017).

Recent studies using MD simulations have successfully described the behaviors of ANOs (Bethel and Grabe, 2016; Le et al., 2019; Yu et al., 2019). Our MD simulations did not include phospholipids or the whole protein structure, and the total simulation time was relatively short for performing in-depth analyses of the system, making our conclusions from the MD simulations very limited. However, considering that our simulation results are in good agreement with the patch-clamp results, we carefully claim that the results from our MD simulations likely reflect reality to some extent.

Delayed activation in the whole-cell patch-clamp configuration is a unique characteristic of ANO6 (Grubb et al., 2013; Kim et al., 2015; Liang and Yang, 2021; Lin et al., 2018; 2019; Scudieri et al., 2015). This characteristic has not been noted in other members of the ANO family, and the precise underlying mechanism remains unclear, although several cytosolic factors, including actin cytoskeleton and Mg-ATP, are known to be involved (Lin et al., 2018). Inactivation of the ANO6 channel is associated with PIP<sub>2</sub> depletion (Ye et al., 2018). In our experiments, ANO6 and ANO6-1-6 showed no

difference in delayed activation or inactivation in the whole-cell patch clamp; thus, it is likely that the Nt-CaRes in ANO6 is not related to the actin cytoskeleton, Mg-ATP, or PIP<sub>2</sub>-dependent channel properties. It would be interesting to further study the effects of various cytosolic or membrane proteins on ANO6 channel and scramblase properties (Dhakal and Lee, 2019; Lee and Ahnn, 2020; Park et al., 2020).

ANO6-1-6 showed increased  $\text{Ca}^{2+}$  sensitivity compared with that of ANO6, but it was not as high as that of ANO1, which is around 1  $\mu\text{M}$  (Pedemonte and Galietta, 2014; Tak et al., 2019; Yang et al., 2008). Other unknown mechanisms may be accountable for the remaining difference in  $\text{Ca}^{2+}$  sensitivity, such as additional regulatory sites existing only in ANO1, different interactions with phospholipids, or unknown allosteric effects (Feng et al., 2019; Ko et al., 2020; Xiao et al., 2011; Ye et al., 2018; Yu et al., 2019). Further studies are needed to fully understand the exact mechanisms.

Several papers have been published on the interactions between ANO1 and calmodulin (Jung et al., 2013; Tian et al., 2011; Vocke et al., 2013; Yang et al., 2014). Among these four papers, the calmodulin-binding domains identified by Jung et al. (2013) and Vocke et al. (2013) were found to be conserved in ANO6 sequences (Supplementary Fig. S1A).

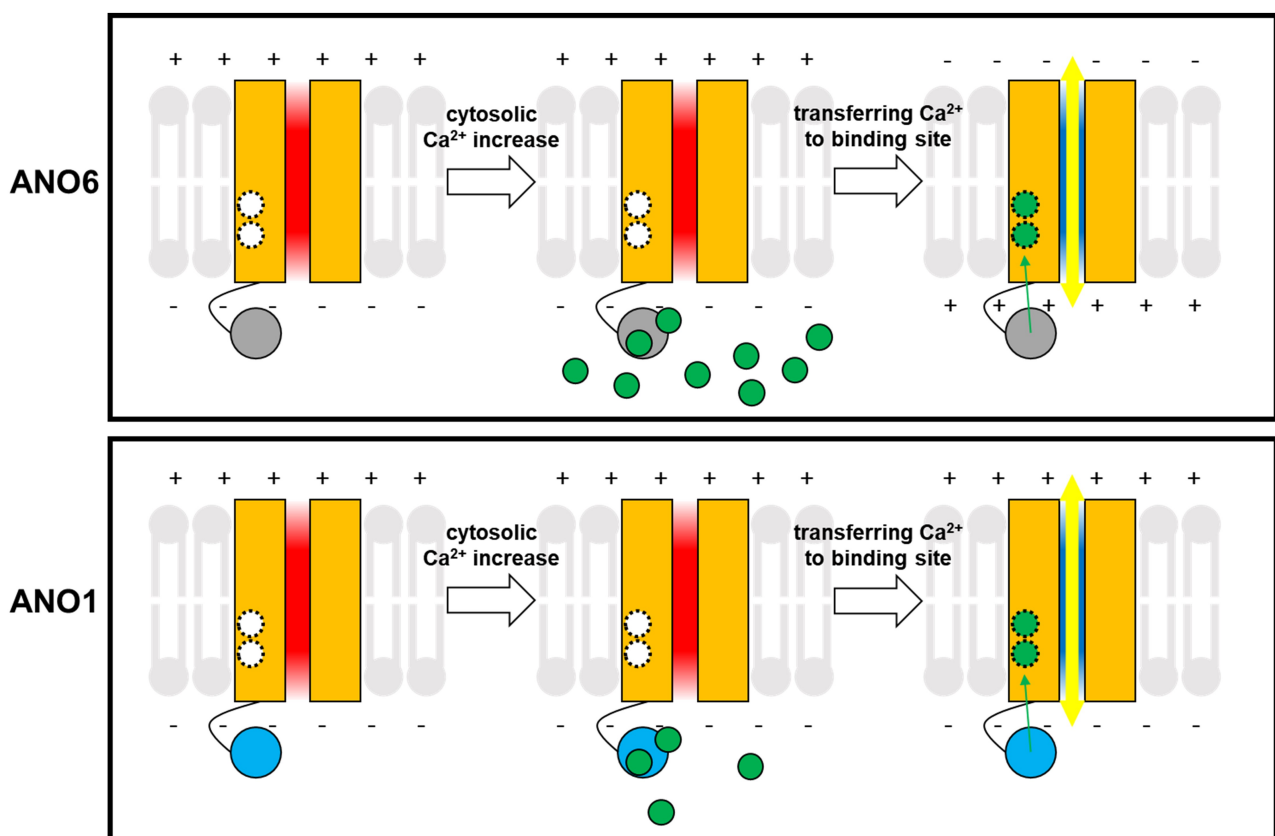


**Fig. 6. Proposed model for Nt-CaRes in ANO6 and ANO1 channel activation.** ANO6 or ANO1 (two orange boxes indicate a single subunit),  $\text{Ca}^{2+}$ -binding site in transmembrane domains (empty circles in ANO6 and ANO1), Nt-CaRes in ANO6 (gray circles), Nt-CaRes in ANO1 (light blue circles), and  $\text{Ca}^{2+}$  (green circles) are indicated. Green arrows indicate the movement of  $\text{Ca}^{2+}$  to the  $\text{Ca}^{2+}$ -binding site. ANO6 and ANO1 pores colored in red indicate a closed channel, while blue indicates an open channel. The yellow arrows indicate ion movements in the open channel.

Interestingly, these calmodulin-binding domains were located in the Nt and were very close to the Nt-CaRes. We therefore investigated the possibility of calmodulin modulation on the Ca<sup>2+</sup> sensitivity of ANO6. We used W-7, a well-known calmodulin inhibitor, and compared Ca<sup>2+</sup> sensitivity with and without W-7 in the whole-cell patch clamp configuration. Regardless of the presence of W-7, Ca<sup>2+</sup> sensitivity remained the same (Supplementary Fig. S1B). Ca<sup>2+</sup> sensitivity without W-7 in the whole-cell patch clamp was 15.23 μM (Hill coefficient = 4.77), and the Ca<sup>2+</sup> sensitivity measured in the presence of W-7 was 17.04 μM (Hill coefficient = 3.28). Normalized currents in 10 μM Ca<sup>2+</sup> were similar without and with W-7 (Supplementary Fig. S1C). Current densities in 10 μM Ca<sup>2+</sup> without W-7 (69.6 ± 9.5 pA/pF) and with W-7 (63.1 ± 9.9 pA/pF) also showed no significant difference (Supplementary Fig. S1D). Based on these results, we believe that calmodulin does not play a role in modulating the Ca<sup>2+</sup> sensitivity of ANO6 and is not related to the Nt-CaRes. In addition, recent studies regarding ANO1 and calmodulin failed to find interactions (Terashima et al., 2013; Tien et al., 2014; Yang and Colecraft, 2016; Yu and Chen, 2015). Thus, further studies are needed to fully address the ongoing debate on the relationship between ANOs and calmodulin.

Based on our experiments, we propose a model to explain the roles of the Nt-CaRes (Fig. 6). Both ANO1 and ANO6 have an Nt-CaRes, although that of ANO6 has low Ca<sup>2+</sup>-binding affinity. Thus, the Nt-CaRes of ANO6 only binds to Ca<sup>2+</sup> at a high cytosolic Ca<sup>2+</sup> concentration. Ca<sup>2+</sup> movement to the Ca<sup>2+</sup>-binding site opens the channel, generating the current in ANO6. Since ANO1 has an Nt-CaRes with high Ca<sup>2+</sup> sensitivity, it can bind to Ca<sup>2+</sup> at a lower concentration; thus, Ca<sup>2+</sup> movement to the Ca<sup>2+</sup>-binding site opens the channel and generates the current in ANO1. Although the exact transferring process of Ca<sup>2+</sup> from the Nt-CaRes to the Ca<sup>2+</sup>-binding site remains unclear, Tak et al. (2019) described the location and function of the Nt-CaRes as the entrance to the Ca<sup>2+</sup>-binding site. Further studies are needed to fully clarify this transferring process.

In conclusion, this study shows that the Nt-CaRes helps Ca<sup>2+</sup> move to the hydrophobic Ca<sup>2+</sup>-binding site of ANO6, which can partially explain the Ca<sup>2+</sup> sensitivity difference between ANO1 and ANO6. The present results provide important and novel evidence regarding the mechanisms underlying ANO6 activation.

Note: Supplementary information is available on the Molecules and Cells website ([www.molcells.org](http://www.molcells.org)).

## ACKNOWLEDGMENTS

This study was supported by the Basic Science Research Program through the National Research Foundation of Korea (NRF) funded by the Ministry of Education of South Korea (No. NRF-2019R111A3A01041391).

## AUTHOR CONTRIBUTIONS

J.H.N. and W.K.K. conceived and supervised the study. J.W.R. and J.H.N. designed the experiments. J.W.R. provided new tools and prepared reagents. J.W.R. and G.E.H. performed experiments and analyzed data. J.W.R. performed simulation

studies. J.W.R., G.E.H., W.K.K., and J.H.N. discussed the results and commented on the manuscript. J.W.R. and G.E.H. wrote and revised the manuscript in consultation with J.H.N.

## CONFLICT OF INTEREST

The authors have no potential conflicts of interest to disclose.

## ORCID

|               |   |
|---------------|---|
| Jae Won Roh   | <a href="https://orcid.org/0000-0002-3692-1739">https://orcid.org/0000-0002-3692-1739</a> |
| Ga Eun Hwang  | <a href="https://orcid.org/0000-0001-5797-455X">https://orcid.org/0000-0001-5797-455X</a> |
| Woo Kyung Kim | <a href="https://orcid.org/0000-0003-0359-3967">https://orcid.org/0000-0003-0359-3967</a> |
| Joo Hyun Nam  | <a href="https://orcid.org/0000-0001-8300-6974">https://orcid.org/0000-0001-8300-6974</a> |

## REFERENCES

- Alvadia, C., Lim, N.K., Clerico Mosina, V., Oostergertel, G.T., Dutzler, R., and Paulino, C. (2019). Cryo-EM structures and functional characterization of the murine lipid scramblase TMEM16F. *Elife* 8, e44365.
- Benkert, P., Kunzli, M., and Schwede, T. (2009). QMEAN server for protein model quality estimation. *Nucleic Acids Res.* 37(Web Server issue), W510-W514.
- Bethel, N.P. and Grabe, M. (2016). Atomistic insight into lipid translocation by a TMEM16 scramblase. *Proc. Natl. Acad. Sci. U. S. A.* 113, 14049-14054.
- Brunner, J.D., Lim, N.K., Schenck, S., Duerst, A., and Dutzler, R. (2014). X-ray structure of a calcium-activated TMEM16 lipid scramblase. *Nature* 516, 207-212.
- Caputo, A., Caci, E., Ferrera, L., Pedemonte, N., Barsanti, C., Sondo, E., Pfeffer, U., Ravazzolo, R., Zegarra-Moran, O., and Galietta, L.J. (2008). TMEM16A, a membrane protein associated with calcium-dependent chloride channel activity. *Science* 322, 590-594.
- Dang, S., Feng, S., Tien, J., Peters, C.J., Bulkley, D., Lolicato, M., Zhao, J., Zuberbuhler, K., Ye, W., Qi, L., et al. (2017). Cryo-EM structures of the TMEM16A calcium-activated chloride channel. *Nature* 552, 426-429.
- Darden, T., York, D., and Pedersen, L. (1993). Particle mesh Ewald: An  $N \log(N)$  method for Ewald sums in large systems. *J. Chem. Phys.* 98, 10089-10092.
- Dhakal, S. and Lee, Y. (2019). Transient receptor potential channels and metabolism. *Mol. Cells* 42, 569-578.
- Ehlen, H.W., Chinenkova, M., Moser, M., Munter, H.M., Krause, Y., Gross, S., Brachvogel, B., Wuelling, M., Kornak, U., and Vortkamp, A. (2013). Inactivation of anoctamin-6/Tmem16f, a regulator of phosphatidylserine scrambling in osteoblasts, leads to decreased mineral deposition in skeletal tissues. *J. Bone Miner. Res.* 28, 246-259.
- Falzone, M.E., Malvezzi, M., Lee, B.C., and Accardi, A. (2018). Known structures and unknown mechanisms of TMEM16 scramblases and channels. *J. Gen. Physiol.* 150, 933-947.
- Feng, S., Dang, S., Han, T.W., Ye, W., Jin, P., Cheng, T., Li, J., Jan, Y.N., Jan, L.Y., and Cheng, Y. (2019). Cryo-EM studies of TMEM16F calcium-activated ion channel suggest features important for lipid scrambling. *Cell Rep.* 28, 567-579.e4.
- Grabarek, Z. (2006). Structural basis for diversity of the EF-hand calcium-binding proteins. *J. Mol. Biol.* 359, 509-525.
- Grubb, S., Poulsen, K.A., Juul, C.A., Kyed, T., Klausen, T.K., Larsen, E.H., and Hoffmann, E.K. (2013). TMEM16F (Anoctamin 6), an anion channel of delayed Ca<sup>2+</sup> activation. *J. Gen. Physiol.* 141, 585-600.
- Harper, M.T. and Poole, A.W. (2013). Chloride channels are necessary for full platelet phosphatidylserine exposure and procoagulant activity. *Cell Death Dis.* 4, e969.
- Hoover, W.G. (1985). Canonical dynamics: equilibrium phase-space distributions. *Phys. Rev. A Gen. Phys.* 31, 1695-1697.

- Huang, J., Rauscher, S., Nawrocki, G., Ran, T., Feig, M., de Groot, B.L., Grubmuller, H., and MacKerell, A.D., Jr. (2017). CHARMM36m: an improved force field for folded and intrinsically disordered proteins. *Nat. Methods* 14, 71-73.
- Humphrey, W., Dalke, A., and Schulter, K. (1996). VMD: visual molecular dynamics. *J. Mol. Graph.* 14, 33-38, 27-28.
- Jorgensen, W.L., Chandrasekhar, J., Madura, J.D., Impey, R.W., and Klein, M.L. (1983). Comparison of simple potential functions for simulating liquid water. *J. Chem. Phys.* 79, 926-935.
- Jung, J., Nam, J.H., Park, H.W., Oh, U., Yoon, J.H., and Lee, M.G. (2013). Dynamic modulation of ANO1/TMEM16A  $\text{HCO}_3^-$  permeability by  $\text{Ca}^{2+}$ /calmodulin. *Proc. Natl. Acad. Sci. U. S. A.* 110, 360-365.
- Kim, H.J., Jun, I., Yoon, J.S., Jung, J., Kim, Y.K., Kim, W.K., Kim, B.J., Song, J., Kim, S.J., Nam, J.H., et al. (2015). Selective serotonin reuptake inhibitors facilitate ANO6 (TMEM16F) current activation and phosphatidylserine exposure. *Pflugers Arch.* 467, 2243-2256.
- Ko, W., Jung, S.R., Kim, K.W., Yeon, J.H., Park, C.G., Nam, J.H., Hille, B., and Suh, B.C. (2020). Allosteric modulation of alternatively spliced  $\text{Ca}^{2+}$ -activated  $\text{Cl}^-$  channels TMEM16A by PI(4,5)P2 and CaMKII. *Proc. Natl. Acad. Sci. U. S. A.* 117, 30787-30798.
- Kunzelmann, K., Nilius, B., Owsianik, G., Schreiber, R., Ousingsawat, J., Sirianant, L., Wanitchakool, P., Bevers, E.M., and Heemskerk, J.W. (2014). Molecular functions of anoctamin 6 (TMEM16F): a chloride channel, cation channel, or phospholipid scramblase? *Pflugers Arch.* 466, 407-414.
- Le, S.C., Jia, Z., Chen, J., and Yang, H. (2019). Molecular basis of PIP<sub>2</sub>-dependent regulation of the  $\text{Ca}^{2+}$ -activated chloride channel TMEM16A. *Nat. Commun.* 10, 3769.
- Lee, J., Cheng, X., Swails, J.M., Yeom, M.S., Eastman, P.K., Lemkul, J.A., Wei, S., Buckner, J., Jeong, J.C., Qi, Y., et al. (2016). CHARMM-GUI input generator for NAMD, GROMACS, AMBER, OpenMM, and CHARMM/OpenMM simulations using the CHARMM36 additive force field. *J. Chem. Theory Comput.* 12, 405-413.
- Lee, S.K. and Ahnn, J. (2020). Regulator of calcineurin (RCAN): beyond Down syndrome critical region. *Mol. Cells* 43, 671-685.
- Liang, P. and Yang, H. (2021). Molecular underpinning of intracellular pH regulation on TMEM16F. *J. Gen. Physiol.* 153, e202012704.
- Lin, H., Jun, I., Woo, J.H., Lee, M.G., Kim, S.J., and Nam, J.H. (2019). Temperature-dependent increase in the calcium sensitivity and acceleration of activation of ANO6 chloride channel variants. *Sci. Rep.* 9, 6706.
- Lin, H., Roh, J., Woo, J.H., Kim, S.J., and Nam, J.H. (2018). TMEM16F/ANO6, a  $\text{Ca}^{2+}$ -activated anion channel, is negatively regulated by the actin cytoskeleton and intracellular MgATP. *Biochem. Biophys. Res. Commun.* 503, 2348-2354.
- Nosé, S. (1984). A unified formulation of the constant temperature molecular dynamics methods. *J. Chem. Phys.* 81, 511-519.
- Park, W.J., Song, J.H., Kim, G.T., and Park, T.S. (2020). Ceramide and sphingosine 1-phosphate in liver diseases. *Mol. Cells* 43, 419-430.
- Paulino, C., Kalienkova, V., Lam, A.K.M., Neldner, Y., and Dutzler, R. (2017). Activation mechanism of the calcium-activated chloride channel TMEM16A revealed by cryo-EM. *Nature* 552, 421-425.
- Pedemonte, N. and Galiotta, L.J. (2014). Structure and function of TMEM16 proteins (anoctamins). *Physiol. Rev.* 94, 419-459.
- Pettersen, E.F., Goddard, T.D., Huang, C.C., Couch, G.S., Greenblatt, D.M., Meng, E.C., and Ferrin, T.E. (2004). UCSF Chimera--a visualization system for exploratory research and analysis. *J. Comput. Chem.* 25, 1605-1612.
- Phillips, J.C., Braun, R., Wang, W., Gumbart, J., Tajkhorshid, E., Villa, E., Chipot, C., Skeel, R.D., Kale, L., and Schulter, K. (2005). Scalable molecular dynamics with NAMD. *J. Comput. Chem.* 26, 1781-1802.
- Ryckaert, J.P., Ciccotti, G., and Berendsen, H.J.C. (1977). Numerical integration of the cartesian equations of motion of a system with constraints: molecular dynamics of n-alkanes. *J. Comput. Phys.* 23, 321-341.
- Schroeder, B.C., Cheng, T., Jan, Y.N., and Jan, L.Y. (2008). Expression cloning of TMEM16A as a calcium-activated chloride channel subunit. *Cell* 134, 1019-1029.
- Schwede, T., Kopp, J., Guex, N., and Peitsch, M.C. (2003). SWISS-MODEL: an automated protein homology-modeling server. *Nucleic Acids Res.* 31, 3381-3385.
- Scudieri, P., Caci, E., Venturini, A., Sondo, E., Pianigiani, G., Marchetti, C., Ravazzolo, R., Pagani, F., and Galiotta, L.J. (2015). Ion channel and lipid scramblase activity associated with expression of TMEM16F/ANO6 isoforms. *J. Physiol.* 593, 3829-3848.
- Soulard, C., Salsac, C., Mouzat, K., Hilaire, C., Roussel, J., Mezghrani, A., Lumbroso, S., Raoul, C., and Scamps, F. (2020). Spinal motoneuron TMEM16F acts at C-boutons to modulate motor resistance and contributes to ALS pathogenesis. *Cell Rep.* 30, 2581-2593.e7.
- Suzuki, J., Umeda, M., Sims, P.J., and Nagata, S. (2010). Calcium-dependent phospholipid scrambling by TMEM16F. *Nature* 468, 834-838.
- Tak, M.H., Jang, Y., Son, W.S., Yang, Y.D., and Oh, U. (2019). EF-hand like region in the N-terminus of anoctamin 1 modulates channel activity by  $\text{Ca}^{2+}$  and voltage. *Exp. Neurobiol.* 28, 658-669.
- Terashima, H., Picollo, A., and Accardi, A. (2013). Purified TMEM16A is sufficient to form  $\text{Ca}^{2+}$ -activated  $\text{Cl}^-$  channels. *Proc. Natl. Acad. Sci. U. S. A.* 110, 19354-19359.
- Tian, Y., Kongsuphol, P., Hug, M., Ousingsawat, J., Witzgall, R., Schreiber, R., and Kunzelmann, K. (2011). Calmodulin-dependent activation of the epithelial calcium-dependent chloride channel TMEM16A. *FASEB J.* 25, 1058-1068.
- Tien, J., Peters, C.J., Wong, X.M., Cheng, T., Jan, Y.N., Jan, L.Y., and Yang, H. (2014). A comprehensive search for calcium binding sites critical for TMEM16A calcium-activated chloride channel activity. *Elife* 3, e02772.
- Vocke, K., Dauner, K., Hahn, A., Ulbrich, A., Broecker, J., Keller, S., Frings, S., and Mohrlen, F. (2013). Calmodulin-dependent activation and inactivation of anoctamin calcium-gated chloride channels. *J. Gen. Physiol.* 142, 381-404.
- Whitlock, J.M. and Hartzell, H.C. (2017). Anoctamins/TMEM16 proteins: chloride channels flirting with lipids and extracellular vesicles. *Annu. Rev. Physiol.* 79, 119-143.
- Wu, N., Cernysiov, V., Davidson, D., Song, H., Tang, J., Luo, S., Lu, Y., Qian, J., Gyurova, I.E., Waggoner, S.N., et al. (2020). Critical role of lipid scramblase TMEM16F in phosphatidylserine exposure and repair of plasma membrane after pore formation. *Cell Rep.* 30, 1129-1140.e5.
- Xiao, Q., Yu, K., Perez-Cornejo, P., Cui, Y., Arreola, J., and Hartzell, H.C. (2011). Voltage- and calcium-dependent gating of TMEM16A/Ano1 chloride channels are physically coupled by the first intracellular loop. *Proc. Natl. Acad. Sci. U. S. A.* 108, 8891-8896.
- Yang, H., Kim, A., David, T., Palmer, D., Jin, T., Tien, J., Huang, F., Cheng, T., Coughlin, S.R., Jan, Y.N., et al. (2012). TMEM16F forms a  $\text{Ca}^{2+}$ -activated cation channel required for lipid scrambling in platelets during blood coagulation. *Cell* 151, 111-122.
- Yang, T. and Colecraft, H.M. (2016). Calmodulin regulation of TMEM16A and 16B  $\text{Ca}^{2+}$ -activated chloride channels. *Channels (Austin)* 10, 38-44.
- Yang, T., Hendrickson, W.A., and Colecraft, H.M. (2014). Preassociated apocalmodulin mediates  $\text{Ca}^{2+}$ -dependent sensitization of activation and inactivation of TMEM16A/16B  $\text{Ca}^{2+}$ -gated  $\text{Cl}^-$  channels. *Proc. Natl. Acad. Sci. U. S. A.* 111, 18213-18218.
- Yang, Y.D., Cho, H., Koo, J.Y., Tak, M.H., Cho, Y., Shim, W.S., Park, S.P., Lee, J., Lee, B., Kim, B.M., et al. (2008). TMEM16A confers receptor-activated calcium-dependent chloride conductance. *Nature* 455, 1210-1215.
- Ye, W., Han, T.W., Nassar, L.M., Zubia, M., Jan, Y.N., and Jan, L.Y. (2018). Phosphatidylinositol-(4, 5)-bisphosphate regulates calcium gating of

small-conductance cation channel TMEM16F. Proc. Natl. Acad. Sci. U. S. A. 115, E1667-E1674.

Yu, K., Jiang, T., Cui, Y., Tajkhorshid, E., and Hartzell, H.C. (2019). A network of phosphatidylinositol 4,5-bisphosphate binding sites regulates gating of the Ca<sup>2+</sup>-activated Cl<sup>-</sup> channel ANO1 (TMEM16A). Proc. Natl. Acad. Sci. U. S. A. 116, 19952-19962.

Yu, Y. and Chen, T.Y. (2015). Purified human brain calmodulin does not alter the bicarbonate permeability of the ANO1/TMEM16A channel. J.

Gen. Physiol. 145, 79-81.

Zaitseva, E., Zaitsev, E., Melikov, K., Arakelyan, A., Marin, M., Villasmil, R., Margolis, L.B., Melikyan, G.B., and Chernomordik, L.V. (2017). Fusion stage of HIV-1 entry depends on virus-induced cell surface exposure of phosphatidylserine. Cell Host Microbe 22, 99-110.e7.

Zhang, Y., Le, T., Grabau, R., Mohseni, Z., Kim, H., Natale, D.R., Feng, L., Pan, H., and Yang, H. (2020). TMEM16F phospholipid scramblase mediates trophoblast fusion and placental development. Sci. Adv. 6, eaba0310.